# Optimization of carrier-depletion silicon optical phase shifter

© E.A. Lavrukhina[1], D.S. Pashin[1], A.V. Nezhdanov[1], K.V. Sidorenko[1], P.V. Volkov[2], A.I. Bobrov[1]

[1] Physical and Technical Research Institute, National Research State University of Nizhny Novgorod, 603022 Nizhny Novgorod, Russia
[2] Institute of Physics of Microstructures, Russian Academy of Sciences, 603950 Nizhny Novgorod, Russia

E-mail: ekaterina.a.lavrukhina@gmail.com

*Received March 26, 2025*
*Revised March 31, 2025*
*Accepted April 3, 2025*

The optimization of the cross-sectional geometry and doping concentrations of the $p-n$ junction in an electro-optic phase shifter, based on the depletion of free carriers in a silicon waveguide, has been performed using the gradient descent method. The configuration obtained through numerical simulation achieves a balance between phase shift efficiency and propagation loss. Additionally, a range of geometrical parameters ensuring single-mode operation in highly doped rib waveguides has been identified. The proposed optimization methodology and resulting findings offer valuable insights for the design of integrated photonic devices.

**Keywords:** silicon photonics, electro-optic phase shifters, silicon-on-insulator, free carrier plasma dispersion effect, single-mode rib optical waveguide.

DOI: 10.61011/SC.2025.01.61070.7693

## 1. Introduction

The amount of information transmitted via the Internet has been growing steadily since the time when the Internet appeared, thus, necessitating an increase in the capacity of communication links [1]. This problem may be solved by silicon photonic devices that surpass electrical systems both in energy efficiency and data rate [2]. These devices are compatible with the complementary metal–oxide–semiconductor (CMOS) manufacturing processes [3,4], have low energy consumption, good scalability and potential for monolithic photonic–electronic integration. These advantages contributed to the explosive development of electro-optic (EO) modulators using the Mach–Zehnder interferometer (MZI) architecture [4–7], with phase shifters playing a key role in their design to ensure carrier signal modulation [8]. Silicon features weakly manifested traditional EO mechanisms such as the Pockels and Franz–Keldysh effects [9]. An alternative approach involves employment of the EO effect of free-carrier plasma dispersion [10,11]. To implement this approach, a heavily-doped $p-n$ junction is created in the phase shifter and integrated in the partially etched waveguide [12]. The applied electric field changes the density of free carriers (electrons and holes), affecting the complex refractive index of the material and leading to a phase shift of the optical signal propagating in the waveguide. However, this method is accompanied by an increase in optical loss at high concentrations of free carriers.

There are currently three main mechanisms for implementing the free-carrier plasma dispersion phase shifter [8]: injection of carriers in the $p-i-n$ junction at direct bias voltage [13,14], carrier depletion of the $p-n$ junction with reverse bias voltage [15] and charge accumulation in the metal–dielectric–semiconductor structure [12,16]. The first of the above-mentioned approaches has the highest efficiency [17], compact size and low free carrier absorption loss owing to the presence of an intrinsic region in the waveguide, which, however, reduces the bandwidth to hundreds of MHz due to slow recombination of holes and electrons [18,19]. The third approach is technologically difficult and requires using lithographic processes with a resolution of a few nanometers [20,21]. As a result, one of the widely used approaches in silicon photonics involves phase shifters based on free-carrier depletion of an optical waveguide due to the ease of fabrication [22,23] and high operating speed with a bandwidth up to tens of GHz. This makes them suitable for devices requiring quick response such as Mach–Zehnder interferometers [5]. However, depletion phase shifters also have some restrictions, which limit their performance compared to the carrier injection/accumulation designs [1]. The main restriction is associated with small variations of refractive index that may result from the decrease in carrier density, which limits the phase shift efficiency [10].

To date, various free-carrier-depletion-based phase shifter designs have been developed [23]. Special attention is given to the $p-n$ junctions shifted off the center of the optical waveguide [24–28] to improve phase shift efficiency and reduce free-carrier absorption loss [10]. Configurations with PIPIN junctions [29,30], *L*- and *U*-shaped junctions [31,32] and alternating $p-n$ junctions throughout the waveguide [33–36] are also proposed. The search for an optimum $p-n$ junction configuration for depletion phase shifters to minimize the loss, to provide a wide bandwidth, and to achieve relatively high phase shift efficiency is still a critical task in silicon photonics [37].

This work makes an effort to find the optimum balance between the phase shift efficiency and free-carrier absorp-

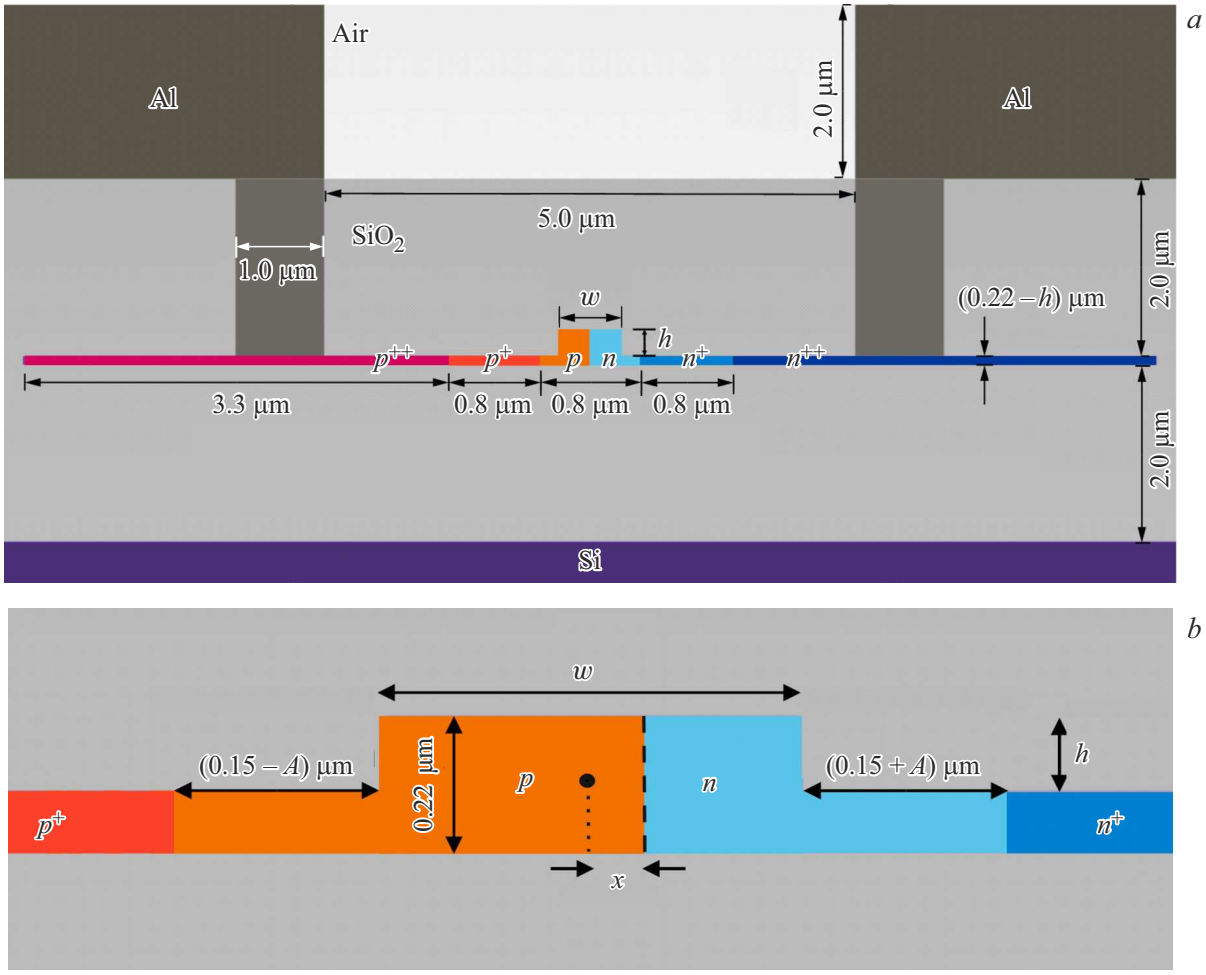


**Figure 1.** *a* — cross-section layout of the free-carrier-depletion-based EO phase shifter (not to scale). *b* — enlarged view of the partially etched waveguide, where $w$, $h$, $A$, $x$, $p$, $n$ indicate waveguide dimensions and dopant concentrations used in the optimization process.

tion loss in phase shifters. A mathematical method for optimizing dimensions and concentrations of phase shifter dopants is proposed. Optimization is performed by finding a local minimum of a function taking into account the phase shift efficiency and optical loss. The optimum configuration of the studied structure was found during numerical simulation. In addition, single-mode condition criteria for partially etched waveguides are discussed to determine the permissible dimension range for keeping the single-mode condition.

## 2. Silicon electro-optic phase shifter model

Configuration of an EO phase shifter cross-section as shown in Figure 1, *a*, is studied. The structure is simulated on the silicon-on-insulator platform with the active silicon layer thickness of $0.22\,\mu$m and a $2\,\mu$m $SiO_2$ insulator, which meets the standard requirements for silicon photonic integrated circuits [4]. The active region of the phase shifter includes a partially etched waveguide with the free-carrier-depletion-based $p{-}n$ junction. Heavily doped regions $(p^{++}/n^{++})$ with a concentration of $2 \cdot 10^{20}\,\mathrm{cm}^{-3}$ located at a distance of $1.2\,\mu$m from the center of the waveguide are connected to aluminum electrodes to form ohmic contacts and apply reverse bias. This arrangement minimizes the overlap between the optical mode and heavily doped regions to reduce propagation loss. Intermediate regions $(p^{+}/n^{+})$ with a dopant concentration of $2 \cdot 10^{18}\,\mathrm{cm}^{-3}$ are placed at $0.4\,\mu$m from the center of the waveguide to increase the bandwidth [38]. The simulation employed uniform doping throughout the cross-section of the doped waveguide regions with sharp boundaries between them.

Figure 1, *b* schematically shows an enlarged view of the cross-section of the active phase shifter region. Parameters to be optimized are shown here: rib width $(w)$, partial etching depth $(h)$, distance from the $p^{+}/n^{+}$ regions to the waveguide rib $(A)$, shift of the $p{-}n$ junction off the center of the waveguide $(x)$, and dopant concentrations in the $p/n$ regions $(p, n)$. The rib width $(w)$ and partial etching depth $(h)$ define the single-mode condition of the waveguide, free-

carrier absorption loss and sidewall roughness loss. $A$, $x$, $p$ and $n$ affect the phase shifter efficiency device compactness, and optical loss. Lumerical CHARGE and MODE software modules were used for the numerical simulation. CHARGE solver was used to calculate the free carrier concentration profiles in the phase shifter cross-section with $w$, $h$, $A$, $x$, $p$, $n$ and bias voltages varied from 0 to $-4$ V. The resulting distributions were exported to the MODE solver to estimate the phase shift and propagation loss.

## 3. Method for optimizing the main parameters of a phase shifter

Gradient descent is one of the main numerical optimization methods widely used for finding local minima of differentiable functions. This iterative algorithm is based on consecutive motion in direction opposite to the target function gradient to ensure the motion along the fastest decrease path [39].

To achieve the balance between optical losses and variation of the waveguide's refractive index during depletion, a target function defined as the product of optical loss and phase shifter efficiency $F = (\alpha_{pn} + \alpha_0)V_\pi L_\pi$. Here, $\alpha_{pn}$ denotes free-carrier absorption loss, $\alpha_0$ defines passive sidewall roughness loss during dry etching of the waveguide that is assumed equal to 1 dB/cm [40]. $L_\pi$ is a length required to provide a phase shift by $\pi$ between a carrier wave going through the phase shifter at zero voltage and the same wave when the voltage $V_\pi$ is applied. $V_\pi L_\pi$ characterizes the phase shifter efficiency and is calculated as follows: $L_\pi = \lambda_0/2\Delta n_{\text{eff}}$, where $\lambda_0 = 1.55\,\mu$m is the carrier signal wavelength, $\Delta n_{\text{eff}}$ is the variation of the effective refractive index of doped silicon during free-carrier depletion.

The local minimum of the target function $F$ is found using the iterative equation:

$$\mathbf{X}_{j+1} = \mathbf{X}_j - ds\nabla F(\mathbf{X}_j), \tag{1}$$

where $\mathbf{X}_{j+1,j}$ is the vector of optimization parameters at step $j+1$ or $j$, respectively, including the geometric dimensions of the waveguide rib and dopant concentration of the $p$–$n$ junction $\{w, h, A, x, p, n\}$; $ds$ is the step size used to update the parameter vector at every iteration, $\nabla F(\mathbf{X}_j)$ is the gradient of $F$ with respect to $\mathbf{X}$. Equation (1) forms a decreasing sequence of function values $F(\mathbf{X}_0) > F(\mathbf{X}_1) > \ldots > F(\mathbf{X}_{n+1})$, which gradually converges to a local minimum. $ds$ defines convergence of the algorithm: too high values may lead to skipping over the local minimum and too low values may lead to deceleration of the optimization process. The gradient descent method is used to find such values of $\mathbf{X}$ that minimize $F$, which reflects the optimum balance between the loss and phase shift efficiency.

## 4. Optimal phase shifter model and single-mode condition

Minimization of $(\alpha_{pn} + \alpha_0)V_\pi L_\pi$ by the gradient descent method using equation (1) provided the optimum phase shifter dimensions and dopant concentrations: $w = 0.5\,\mu$m, $h = 0.15\,\mu$m, $A = 0.04\,\mu$m, $x = 0.03\,\mu$m, $p = 1 \cdot 10^{17}\,\text{cm}^{-3}$, $n = 1 \cdot 10^{17}\,\text{cm}^{-3}$. Figure 2, *a* shows the optimized waveguide cross-section. The resulting structure has the $p$–$n$ junction shifted off the center of the waveguide, where the $p$ type region takes the largest area in the rib cross-section. This agrees with the known results [10], according to which holes change the refractive index more effectively than electrons, thus, requiring an increased area of the $p$ region to increase the phase shift efficiency.

As shown in Figure 2, *b*, when the reverse bias voltage of 4 V is applied, the depletion region induced by the shift of the $p$–$n$ junction is localized within the waveguide rib overlapping the fundamental mode significantly. Thus, the maximum value of $\Delta n_{\text{eff}}$ can be reached at the optimum concentrations of free carriers in the $p/n$ regions minimizing the free-carrier absorption loss and preserving the high efficiency. Fundamental mode localization is shown in Figure 2, *c*.

For this configuration, the expected free-carrier absorption loss of the main mode is 2.5 dB/cm. When the reverse voltage of 4 V is applied, variation of the effective refractive index reaches $1.07 \cdot 10^{-4}$, and the phase shifter length required for the phase shift by $\pi$ is equal to 0.725 cm.

Single-mode condition is one of the prerequisites for proper operation of phase shifters [41–44]. To meet this condition, only one mode with the highest effective refractive index must be able to propagate and should be well localized in the waveguide rib region. Quantitative estimate of mode localization uses the filling factor [43]:

$$\text{filling factor} = \frac{\int\limits_R P(S)dS}{\int\limits_\infty P(S)dS}, \tag{2}$$

where $P(S)$ is the mode power distribution density, and $R$ is the waveguide rib region. The mode is considered to be propagating, if its filling factor exceeds 5% [43,44].

For heavily-doped phase shifters, including the structure with the $p$–$n$ junction as shown in Figure 1, *a*, additional criterion associated with the free-carrier absorption loss may be defined for the propagating mode. The mode amplitude of the electromagnetic field propagated along the waveguide in direction $y$ in a medium with the complex effective refractive index $n_{\text{eff}} + i\kappa_{\text{eff}}$ is proportional to $\sim \exp(-2\pi\kappa_{\text{eff}} y/\lambda_0)$. Waveguide mode propagation loss is calculated as follows

$$\alpha = 20\,\frac{2\pi\kappa_{\text{eff}}}{\lambda_0}\,\log_{10}(e), \tag{3}$$

where $\lambda_0 = 1.55\,\mu$m. The mode is considered to be non-propagating, if its power decays by a factor of $\sim 100$

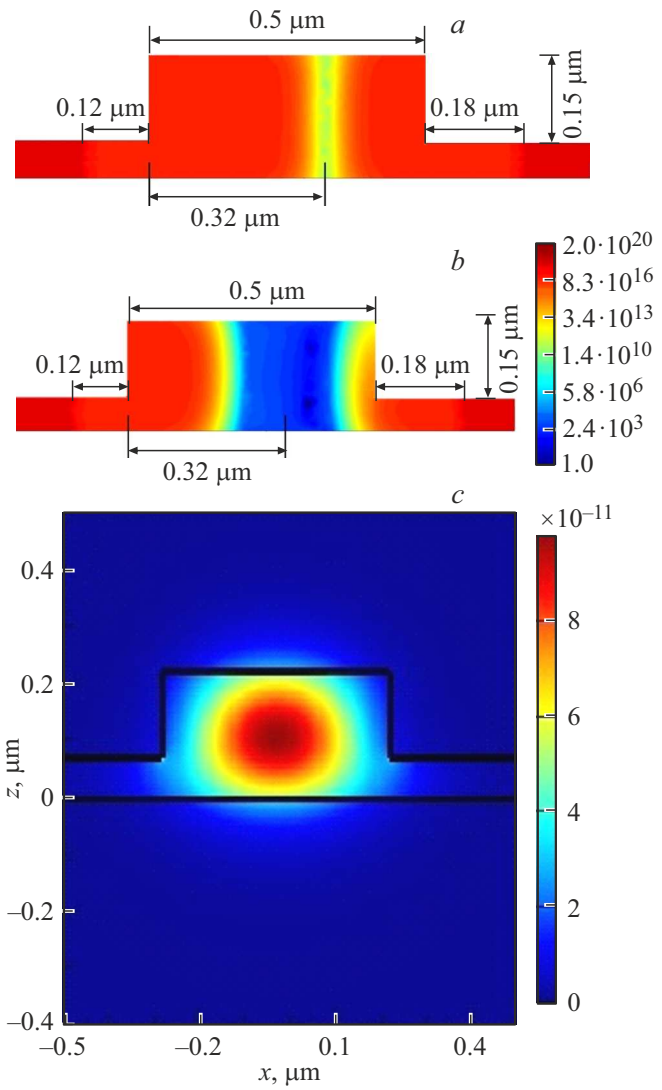


**Figure 2.** *a* — enlarged cross-section view of the rib waveguide with the specified dimensions achieved from the gradient descent optimization. The dopant concentration in the $p/n$ regions is $1 \cdot 10^{17}\,\mathrm{cm}^{-3}$ providing moderate optical loss and sufficient width of the depletion region. The free-carrier concentration distribution at zero bias is shown in color. *b* — free-carrier concentration distribution (on a logarithmic scale) under a reverse bias of 4 V, showing depletion across the $p{-}n$ junction. *c* — distribution of the waveguide fundamental mode energy at 1.55 $\mu$m.

during propagation at the length $L$. Then the threshold loss from (3) will be written as

$$\alpha^* \approx \frac{20\,\mathrm{dB}}{L}. \qquad (4)$$

Thus, for the typical phase shifter length $L = 0.5$ cm, optical modes are considered to be fully evanescent when the loss is $\geq 40$ dB/cm.

The presented calculations considered only those modes, for which the effective refractive index $n_{\mathrm{eff}}$ exceeded the ambient refractive index $n_c$, in our case $n_c = n_{\mathrm{SiO_2}} = 1.44$ (at $\lambda_0 = 1.55\,\mu$m), which is a necessary condition for full internal reflection. In Figure 3, the single-mode region for both doped and undoped waveguides is shown in grey, the multimode region is shown in black, and the hatched region corresponds to single-mode operation in the doped waveguide and multimode behavior in the undoped one. This feature is caused by the fact that, for particular dimensions, some modes in the doped waveguide localized in the rib undergo considerable free-carrier absorption loss.

Optical characteristics of modes in the phase shifter with the optimum configuration as shown in Figure 2, *a*

| Mode | $n_{\mathrm{eff}}$ | $\alpha_{pn}$, dB/cm | Filling factor, % |
|---|---|---|---|
| 1 | 2.56 | 2.5 | 74 |
| 2 | 2.0 | 63 | 24 |
| 3 | 1.89 | 1132 | 10 |
| 4 | 1.76 | 414 | 32 |

Sometimes equality of the effective refractive index and ambient refractive index is assumed as a cutoff condition. However, in terms of operation of a certain device, modes that are formally propagating, but have high loss, don't affect the operation and can be neglected. While improvement in the mode localization under the rib, when, for example, the etching depth increases, may lead to an increase in higher-order mode loss in doped waveguides, because the largest part of the mode starts propagating in the heavily-doped region.

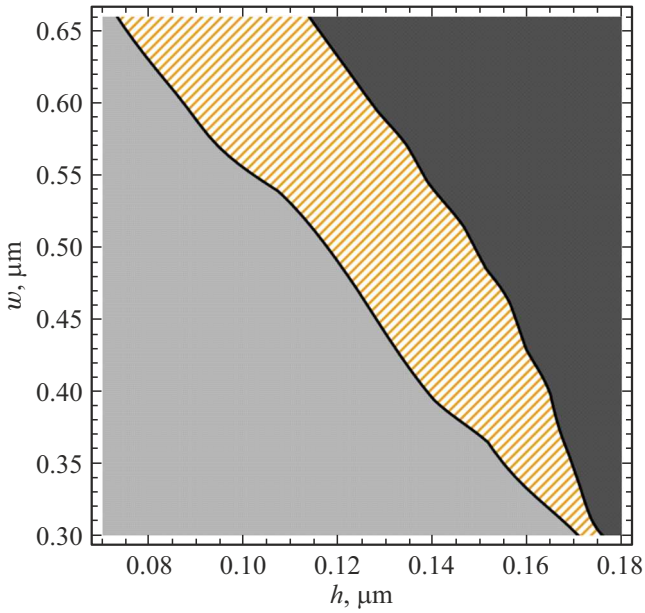


**Figure 3.** Parameter plane of rib width ($w$) and depth ($h$) of the partially etched waveguide. The region corresponding to single-mode operation for both doped and undoped waveguides is shown in grey, the multimode region is shown in black, and the hatched area in between represents a single-mode regime for the doped waveguide and a multimode regime for an undoped waveguide at 1.55 $\mu$m.

Comparison of Figure 3 with previous studies [41–43] on the single-mode regime in undoped partially etched silicon waveguides reveals considerable differences in the behavior of the single-mode condition boundary. This is associated, on the one hand, with the difference in cladding materials and, on the other hand, with the proximity of the studied dimensions to the limit defined by the effective wavelength in silicon $\lambda_0/n_{\mathrm{Si}} \approx 0.447\,\mu$m, where $n_{\mathrm{Si}} = 3.47$ at $\lambda_0 = 1.55\,\mu$m.

For the phase shifter with the optimum configuration obtained by the gradient descent method and shown in Figure 2, *a*, the table shows optical characteristics of the first four modes with the highest $n_{\mathrm{eff}}$ and filling factors exceeding 5%.

It follows from the table that the phase shifter with the optimum configuration operates in a single-mode regime: other modes are either weakly localized in the rib or have free-carrier absorption losses higher than 40 dB/cm, which agrees well with the single-mode criterion as shown in Figure 3.

## 5. Conclusion

This work proposes an approach to optimization of EO silicon phase shifters based on free-carrier-depletion effect. Gradient descent was applied for selecting the optimum cross-section dimensions of the partially etched waveguide and dopant concentrations made it possible to achieve the balance between the phase shift efficiency and free-carrier absorption loss.

The developed structure satisfies the single-mode conditions, as confirmed by the filling factor calculations and additional free-carrier absorption loss criterion ($> 40$ dB/cm) ensuring the effective propagation of the fundamental mode. The optimized configuration demonstrates the free-carrier absorption loss of 2.5 dB/cm and variation of the effective refractive index by $1.07 \cdot 10^{-4}$ when the reverse bias voltage of $V_\pi = 4$ V is applied, while the phase shifter length is $L_\pi = 0.725$ cm.

The proposed phase shifter is a promising candidate for integrated photonics due to the combination of low loss and relatively high efficiency, which makes it suitable for high-speed modulators such as Mach–Zehnder interferometers.

### Funding

Mathematical simulation was supported by the Ministry of Science and Higher Education of the Russian Federation, project No. FSWR-2022-0007. Experimental part of the work was performed within the research program of the National Center of Physics and Mathematics, Topic No. 1 „National Center for Supercomputer Architecture Studies. Phase 2023–2025“.

### Conflict of interest

The authors declare that they have no conflict of interest.

## References

[1] A. Rahim, A. Hermans, B. Wohlfeil, D. Petousi, B. Kuyken, D. Van Thourhout, R. Baets. Adv. Photon., **3** (2), 024003 (2021). https://doi.org/10.1117/1.AP.3.2.024003
[2] Y. Arakawa, T. Nakamura, Y. Urino, T. Fujita. IEEE Commun. Mag., **51** (3), 72 (2013). DOI: 10.1109/MCOM.2013.6476868
[3] G. Sinatkas, T. Christopoulos, O. Tsilipakos, E.E. Kriezis. J. Appl. Phys., **130** (1), 010901 (2021). https://doi.org/10.1063/5.0048712
[4] C.R. Doerr. Front. Phys., **3**, 37 (2015). https://doi.org/10.3389/fphy.2015.00037
[5] A. Liu, L. Liao, D. Rubin, H. Nguyen, B. Ciftcioglu, Y. Chetrit, N. Izhaky, M. Paniccia. Opt. Express, **15** (2), 660 (2007). https://doi.org/10.1364/OE.15.000660
[6] P. Dong, S. Liao, D. Feng, H. Liang, D. Zheng, R. Shafiiha, C.-C. Kung, W. Qian, G. Li, X. Zheng, A.V. Krishnamoorthy, M. Asghari. Opt. Express, **17** (25), 22484 (2009). https://doi.org/10.1364/OE.17.022484
[7] G.V. Treyz, P.G. May, J.M. Halbout. Appl. Phys. Lett., **59** (7), 771 (1991). DOI: 10.1063/1.105338
[8] Y. Kim, J.H. Han, D. Ahn, S. Kim. Micromachines, **12** (6), 625 (2021). https://doi.org/10.3390/mi12060625
[9] R.S. Jacobsen, K.N. Andersen, P.I. Borel, J. Fage-Pedersen, L.H. Frandsen, O. Hansen, M. Kristensen, A.V. Lavrinenko, G. Moulin, H. Ou, C. Peucheret, B. Zsigri, A. Bjarklev. Nature, **441** (7090), 199 (2006). DOI: 10.1038/nature04706
[10] R. Soref, B. Bennett. IEEE J. Quant. Electron., **23** (1), 123 (1987). DOI: 10.1109/JQE.1987.1073206
[11] M. Nedeljkovic, R. Soref, G.Z. Mashanovich. IEEE Photonics J., **3** (6), 1171 (2011). DOI: 10.1109/JPHOT.2011.2171930
[12] L. Liao, D. Samara-Rubio, M. Morse, A. Liu, D. Hodge, D. Rubin, U.D. Keil, T. Franck. Opt. Express, **13** (8), 3129 (2005). https://doi.org/10.1364/OPEX.13.003129
[13] C.K. Tang, G.T. Reed. Electron. Lett., **31** (6), 451 (1995). DOI: 10.1049/EL:19950328
[14] W.M. Green, M.J. Rooks, L. Sekaric, Y.A. Vlasov. Opt. Express, **15** (25), 17106 (2007). https://doi.org/10.1364/OE.15.017106
[15] F.Y. Gardes, G.T. Reed, N.G. Emerson, C.E. Png. Opt. Express, **13** (22), 8845 (2005). https://doi.org/10.1364/OPEX.13.008845
[16] A. Liu, R. Jones, L. Liao, D. Samara-Rubio, D. Rubin, O. Cohen, R. Nicolaescu, M. Paniccia. Nature, **427** (6975), 615 (2004). DOI: 10.1038/nature02310
[17] Q. Xu, B. Schmidt, S. Pradhan, M. Lipson. Nature, **435** (7040), 325 (2005). DOI: 10.1038/nature03569
[18] F. Gan, F.X. Kartner. IEEE Photon. Technol. Lett., **17** (5), 1007 (2005). DOI: 10.1109/LPT.2005.846756
[19] T. Baba, S. Akiyama, M. Imai, T. Usuki. Opt. Express, **23** (26), 32950 (2015). https://doi.org/10.1364/OE.23.032950
[20] J. Fujikata, S. Takahashi, M. Takahashi, M. Noguchi, T. Nakamura, Y. Arakawa. Jpn. J. Appl. Phys., **55** (4S), 04EC01 (2016). DOI: 10.7567/JJAP.55.04EC01
[21] K. Debnath, D.J. Thomson, W. Zhang, A.Z. Khokhar, C. Littlejohns, J. Byers, L. Mastronardi, M.K. Husain, K. Ibukuro, F.Y. Gardes, G.T. Reed, S. Saito. Photonics Res., **6** (5), 373 (2018). https://doi.org/10.1364/PRJ.6.000373
[22] K. Ogawa. Photonics, **11** (6), 535 (2024). https://doi.org/10.3390/photonics11060535

[23] T.G. Reed, G.Z. Mashanovich, F.Y. Gardes, M. Nedeljkovic, Y. Hu, D.J. Thomson, K. Li, P.R. Wilson, S.-W. Chen, S.S. Hsu. Nanophotonics, **3** (4–5), 229 (2014). https://doi.org/10.1515/nanoph-2013-0016
[24] D. Patel, V. Veerasubramanian, S. Ghosh, A. Samani, Q. Zhong, D.V. Plant. Opt. Express, **22** (22), 26788 (2014). https://doi.org/10.1364/OE.22.026788
[25] J. Wang, C. Qiu, H. Li, W. Ling, L. Li, A. Pang, Z. Sheng, A. Wu, X. Wang, S. Zou, F. Gan. J. Lightwave Technol., **31** (24), 4119 (2013). DOI: 10.1109/Jlt.2013.2287671
[26] N.-N. Feng, S. Liao, D. Feng, P. Dong, D. Zheng, H. Liang, R. Shafiiha, G. Li, J.E. Cunningham, A.V. Krishnamoorthy, M. Asghari. Opt. Express, **18** (8), 7994 (2010). https://doi.org/10.1364/OE.18.007994
[27] C.E. Png, M.J. Sun, S.T. Lim, T.Y. Ang, K. Ogawa. IEEE J. Select. Topics Quant. Electron., **22** (6), 99 (2016). DOI: 10.1109/JSTQE.2016.2564648
[28] X. Xiao, H. Xu, X. Li, Z. Li, T. Chu, Y. Yu, J. Yu. Opt. Express, **21** (4), 4116 (2013). https://doi.org/10.1364/OE.21.004116
[29] M. Ziebell, D. Marris-Morini, G. Rasigade, J.-M. Fédéli, P. Crozat, E. Cassan, D. Bouville, L. Vivien. Opt. Express, **20** (10), 10591 (2012). https://doi.org/10.1364/OE.20.010591
[30] X. Tu, T.Y. Liow, J. Song, X. Luo, Q. Fang, M. Yu, G.Q. Lo. Opt. Express, **21** (10), 12776 (2013). https://doi.org/10.1364/OE.21.012776
[31] Y. Kim, T. Jin, Y. Bae. Jpn. J. Appl. Phys., **60** (5), 052002 (2021). DOI: 10.35848/1347-4065/abeedd
[32] Y. Zheng, W.D. Sacher, Y. Huang, J.C. Mikkelsen, Y. Yang, X. Luo, P. Dumais, D. Goodwill, H. Bahrami, P.G.-Q. Lo, E. Bernier, J.K.S. Poon. Opt. Express, **25** (7), 8425 (2017). https://doi.org/10.1364/OE.25.008425
[33] D. Marris-Morini, C. Baudot, J.-M. Fédéli, G. Rasigade, N. Vulliet, A. Souhaité, M. Ziebell, P. Rivallin, S. Olivier, P. Crozat, X. Le Roux, D. Bouville, S. Menezo, F. Bœuf, L. Vivien. Opt. Express, **21** (19), 22471 (2013). https://doi.org/10.1364/OE.21.022471
[34] X. Xiao, X. Li, H. Xu, Y. Hu, K. Xiong, Z. Li. IEEE Photon. Technol. Lett., **24** (19), 1712 (2012). DOI: 10.1109/LPT.2012.2213244
[35] Z.Y. Li, D.X. Xu, W.R. McKinnon, S. Janz, J.H. Schmid, P. Cheben, J.Z. Yu. Opt. Express, **17** (18), 15947 (2009). https://doi.org/10.1364/OE.17.015947
[36] D. Pérez-Galacho, D. Marris-Morini, R. Stoffer, E. Cassan, C. Baudot, T. Korthorst, F. Boeuf, L. Vivien. Opt. Express, **24** (23), 26332 (2016). https://doi.org/10.1364/OE.24.026332
[37] J. Witzens. Proc. IEEE, **106** (12), 2158 (2018). DOI: 10.1109/JPROC.2018.2877636
[38] R. Ding, Y. Liu, Y. Ma, Y. Yang, Q. Li, A. Eu-Jin Lim, G.Q. Lo, K. Bergman, T. Baehr-Jones, M. Hochberg. J. Lightwave Technol., **32** (12), 2240 (2014). DOI: 10.1109/JLT.2014.2323954
[39] A.V. Gasnikov. *Sovremennye chislennye metody optimizatsii. Metod universalnogo gradientnogo spuska* (M., MFTI, 2018). (in Russian). ISBN 978-5-7417-0667-1
[40] K. Debnath, H. Arimoto, M.K. Husain, A. Prasmusinto, A. Al-Attili, R. Petra, H.M.H. Chong, G.T. Reed, S. Saito. Front. Mater., **3**, 10 (2016). https://doi.org/10.3389/fmats.2016.00010
[41] R.A. Soref, J. Schmidtchen, K. Petermann. IEEE J. Quant. Electron., **27** (8), 1971 (1991). DOI: 10.1109/3.83406
[42] O. Powell. J. Lightwave Technol., **20** (10), 1851 (2002). DOI: 10.1109/JLT.2002.804036
[43] H. Huang, K. Liu, B. Qi, V.J. Sorger. J. Lightwave Technol., **34** (16), 3811 (2016). DOI: 10.1109/JLT.2016.2579163
[44] D. Dai, Z. Sheng. J. Opt. Soc. Am. B, **24**, 2853 (2007). https://doi.org/10.1364/JOSAB.24.002853

*Translated by E.Ilinskaya*